ISSN 2072-5981
doi: 10.26907/mrsej

Magnetic Resonance in Solids

Electronic Journal

Volume ***21***
Special Issue ***4***
Paper No ***19407***
1-9 pages
2019

doi: **10.26907/mrsej-19407**

http://mrsej.kpfu.ru
http://mrsej.ksu.ru

Established and published by Kazan University
Endorsed by International Society of Magnetic Resonance (ISMAR)
Registered by Russian Federation Committee on Press (#015140),
August 2, 1996
First Issue appeared on July 25, 1997

"***Magnetic Resonance in Solids. Electronic Journal***" (**MRSej**) is a peer-reviewed, all electronic journal, publishing articles which meet the highest standards of scientific quality in the field of basic research of a magnetic resonance in solids and related phenomena.

Indexed and abstracted by
Web of Science (*ESCI*, Clarivate Analytics, from 2015),
Scopus (Elsevier, from 2012), *RusIndexSC* (*eLibrary*, from 2006), *Google Scholar*,
DOAJ, *ROAD*, *CyberLeninka* (from 2006), *SCImago Journal & Country Rank*, etc.

* In Kazan University the Electron Paramagnetic Resonance (EPR) was discovered by Zavoisky E.K. in 1944.

Ferromagnetic resonance study of the epitaxial VN/$Pd_{0.96}Fe_{0.04}$ thin film heterostructure on MgO substrate

A. Esmaeili[1], W.M. Mohammed[1], I.V. Yanilkin[1], A.I. Gumarov[1], I.R. Vakhitov[1], B.F. Gabbasov[1], A.G. Kiiamov[1], M.N. Aliyev[2], R.V. Yusupov[1,*], L.R. Tagirov[1,3]

[1]Kazan Federal University, Kremlevskaya 18, Kazan 420008, Russia

[2]Baku State University, Z. Khalilov 23, Baku AZ-1148, Azerbaijan

[3]Zavoisky Physical-Technical Institute, FRC "Kazan Scientific Center of RAS", Sibirsky Trakt 10/7, Kazan 420029, Russia

[*]*E-mail: Roman.Yusupov@kpfu.ru*

(Received May 27, 2019; accepted May 28, 2019; published June 6, 2019)

The paper reports on the ferromagnetic resonance (FMR) and magnetometry studies of the epitaxial superconductor/ferromagnet-type thin film heterostructure of VN/$Pd_{0.96}Fe_{0.06}$ on the (001)-oriented MgO substrate. Vanadium nitride layer was deposited by *dc* reactive magnetron sputtering of the V-target in the mixture of the Ar and N_2-gases. Pd-Fe layer was grown by molecular beam deposition in the ultrahigh vacuum conditions. LEED patterns and XRD analysis revealed the "cube-on-cube" epitaxy at both the MgO/VN and VN/$Pd_{0.96}Fe_{0.06}$ interfaces and single crystalline structure of both layers. Ferromagnetic resonance spectra revealed a single absorption line with strong orientation dependence and manifestations of superconductivity of the VN-layer at a temperature of 4.2 K. Magnetic anisotropy constants for the $Pd_{0.96}Fe_{0.06}$ layer were found from the analysis of the orientation dependence of the FMR resonance field and were compared with that of the film of the same composition grown directly on MgO. We find that the tetragonal distortion for $Pd_{0.96}Fe_{0.06}$ on the VN layer is reduced due to a relaxed lattice mismatch with respect to MgO.

PACS: 75.40.Gb, 75.47.Np, 74.25.Nf, 74.70.Ad.

Keywords: palladium-iron alloy, vanadium nitride, epitaxial heterostructure, ferromagnetic resonance, magnetocrystalline anisotropy.

Dedicated to Professor Boris Z. Malkin on the occasion of his 80th birthday

1. Introduction

Potential applications of thin film ferromagnet/superconductor (F/S) heterostructures have led to comprehensive investigations in this field, the most important of them including proximity [1] and Josephson effects [1–5]. Dilute ferromagnetic films with low coercive field have gained significant practical importance due to possibility of their integration into Josephson S/F/S heterostructures [6–11]. Due to low magnetic moment and tunability of the Curie temperature, Cu-Ni and Pd-Fe alloys are the two main candidates that are currently being considered for application in S/F/S heterostructures [4, 11–13]. Thus, Cu-Ni alloy was used in the S/F/S-type junction of Nb/CuNi/Nb to demonstrate the flow of the Josephson supercurrent through the ferromagnetic barrier, as well as the intrinsic inversion of the phase of the superconducting wavefunction across the ferromagnetic link ($0 - \pi$ crossover junction) [14, 15]. Thin films of $Pd_{1-x}Fe_x$ alloys with low iron content x exhibit an anisotropy in the film plane and small coercive field, which makes them ideal candidates for new elements of cryogenic magnetic memory based on the Josephson effect [4, 5, 11]. In these devices, the value of the critical Josephson current is determined by the applied magnetics flux, including the orientation of the magnetization, and thus is tightly related to the magnetic history of the ferromagnetic layer. In [16] the studies of the S/F/S junction with weakly ferromagnetic $Pd_{0.99}Fe_{0.01}$ interlayer were reported that lead to the suggestion of utilizing this material in magnetic switches. Thus, $Pd_{1-x}Fe_x$ alloys are low-temperature soft ferromagnetic materials promising for thin film devices based on S/F/S-type heterostructures.

Important properties that obviously influence the characteristics of heterostructure-based electronic components is the crystallinity of the layers and quality (transparency) of the interfaces. Undoubtedly, an operation of the devices based on polycrystalline layers and of those based on heteroepitaxial structures would differ significantly. Other important differences related to heterostructure crystallinity include reproducibility of characteristics and long-term stability of the elements. A search for S/F layer combinations suitable for heteroepitaxial multilayer structures nowadays therefore is strongly requested.

Recently, we have successfully developed a procedure for high-quality epitaxial $Pd_{1-x}Fe_x$ ($x < 0.10$) film synthesis on the (001)-oriented MgO substrate [17]. The most popular now material for S-layers of S/F/S structures is niobium. There were no reports found on successful epitaxial growth of the Nb thin films on MgO or $SrTiO_3$ because of incommensurability of their lattices. The same holds for the epitaxy between Nb and $Pd_{1-x}Fe_x$. Another attracting class of superconductors is cubic transition metal nitrides. Among those, we find the vanadium nitride (VN) as most suitable for a synthesis of heteroepitaxial S/F/S-structures. It's lattice constant value of 413.4 pm [18] is between that for MgO (421.2 pm) and $Pd_{1-x}Fe_x$ ($\sim$ 388.0 pm [17]) and thus, embedded between the latter two would relax relatively hard epitaxy condition ($\Delta a/a_0 = -7.9\%$) for $Pd_{1-x}Fe_x$/MgO pair. At the same time, the critical temperature of the transition to the superconducting state on the VN (values up to 9.20 K were reported [19]) is almost the same as that of the bulk niobium (9.25 K).

In this paper, we report on the successful synthesis of low-temperature S/F heteroepitaxial thin-film structure VN/$Pd_{0.96}Fe_{0.04}$ on the single-crystal (001)-MgO substrate and present the results of the $Pd_{0.96}Fe_{0.04}$ layer magnetic anisotropy studied with ferromagnetic resonance (FMR) spectroscopy.

2. Sample preparation and characterization techniques

2.1. Sample synthesis

Ultrahigh vacuum setup including the magnetron sputtering (BESTEC, Germany), molecular beam deposition and analytics chambers (SPECS, Germany) was used to synthesize the heterostructure of VN/$Pd_{0.96}Fe_{0.04}$ on MgO. Before the deposition, the chamber was evacuated below 3×10^{-9} mbar. Vanadium nitride film was grown directly on the annealed in the UHV at 800°C for 5 minutes epi-ready MgO (001) substrate by the reactive *dc* magnetron sputtering technique. Vanadium metal disc with the purity of 99.995% served as a target, and the atmosphere in the chamber was composed of Ar as a plasma gas and nitrogen (N_2) as a reactive gas with the pre-calibrated rates of flow of 12 cm^3/min and 8 cm^3/min, respectively. The working pressure was kept at 6×10^{-3} mbar. The magnetron power was fixed at 100 W. The substrate temperature during the deposition was 500°C. Film thickness was measured with the stylus Bruker DektakXT profilometer *ex situ* after the whole structure deposition, and the VN layer was found 15-nm thick. For synthesis of the heterostructure, a thin $Pd_{0.96}Fe_{0.04}$ film with a thickness of 20 nm was epitaxially grown on the VN layer following the three-step procedure [17] after movement of the sample holder to the molecular beam epitaxy (MBE) chamber without breaking the UHV conditions. At every step, the *in situ* low-energy electron diffraction (LEED) pattern was observed (see Fig. 1). Sharpness of the LEED patterns confirms that the good crystallinity of every layer in the heteroepitaxial VN/$Pd_{0.96}Fe_{0.04}$ on MgO has been achieved.

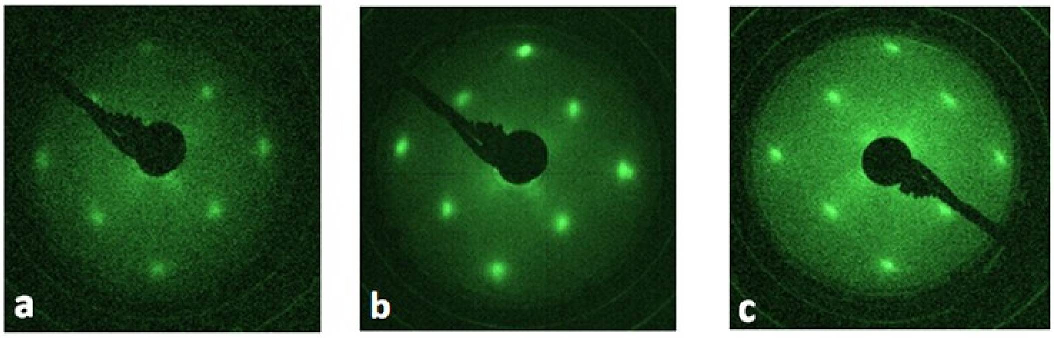

Figure 1. LEED patterns of (a) MgO (001), (b) VN (15 nm) on MgO, and (c) VN (15 nm)/PdFe (20 nm) on MgO; the electrons energy is 140 eV.

2.2. Experimental details

Elemental composition of the grown layers was defined with the X-ray photoelectron spectroscopy (XPS). XPS spectra were measured *in situ* in the ultrahigh vacuum analytical chamber (base pressure $\sim 3 \times 10^{-10}$ mbar) with the Mg-Kα X-ray source operated at 12.5 kV. X-ray diffraction patterns were measured in the Bragg-Brentano geometry with Bruker D8 Advance diffractometer equipped with the Cu-Kα (the wavelength $\lambda = 1.5418$ Å) source and Euler cradle for sample rotation. The vibrating sample magnetometry (VSM) option of the Quantum Design PPMS-9 system was used to measure the $M(B,T)$ dependencies. Commercial *cw* X-band ($\sim$ 9.4 GHz) Bruker ESP300 EPR spectrometer equipped with a standard ER4102ST TE_{102}-mode rectangular cavity was utilized for FMR spectra recording. Sample temperature was controlled using the Oxford Instruments ESR9 continuous helium flow cryostat.

3. Sample characterization

3.1. XPS analysis

The chemical composition of the constituent elements of the top surface of the heterostructure was verified with XPS analysis. Figure 2 shows the XPS spectrum of the top $Pd_{0.96}Fe_{0.04}$ thin film layer. The spectrum of Pd $3d$-electrons reveals two peaks at 341 eV and 335 eV originating from the Pd-$3d_{3/2}$ and Pd-$3d_{5/2}$ states, respectively [20]. For iron, the binding energies of 721.5 eV and 708.7 eV correspond to Fe-$2p_{1/2}$ and Fe-$3d_{3/2}$ states [20]. It is clearly seen from the spectrum that no contamination can be found at the surface of the heterostructure. No signatures of V or N could be detected which points out that the VN was conformally covered with the $Pd_{0.96}Fe_{0.04}$ alloy. The actual atomic composition estimated from the high-resolution spectra of the Pd-$3d_{5/2}$ and Fe-$2p_{3/2}$ electrons was defined as $Pd_{0.957}Fe_{0.043}$ and turned out to be in a good agreement with that pre-determined by the preliminary calibrated deposition rates [17].

3.2. Crystal structure of the layers

X-ray diffraction pattern of the resulting VN/$Pd_{0.96}Fe_{0.04}$ heterostructure measured in the Bragg-Brentano geometry is presented in Fig. 3. Distinct out-of-plane (002) maxima for the substrate and heterostructure layers are clearly seen and are found at the expected 2θ-values. Relatively large width of the diffraction maxima of the VN and $Pd_{0.96}Fe_{0.04}$ layers is in full agreement with its value predicted by the Scherrer relation [17] and thus is due to their nanometer-scale thickness. In total, XRD data combined with mutually coherent LEED patterns (Fig. 1) reveal high crystallinity and "cube-on-cube" epitaxy of the VN/$Pd_{0.96}Fe_{0.04}$ heterostructure on the single-crystal MgO (001) substrate.

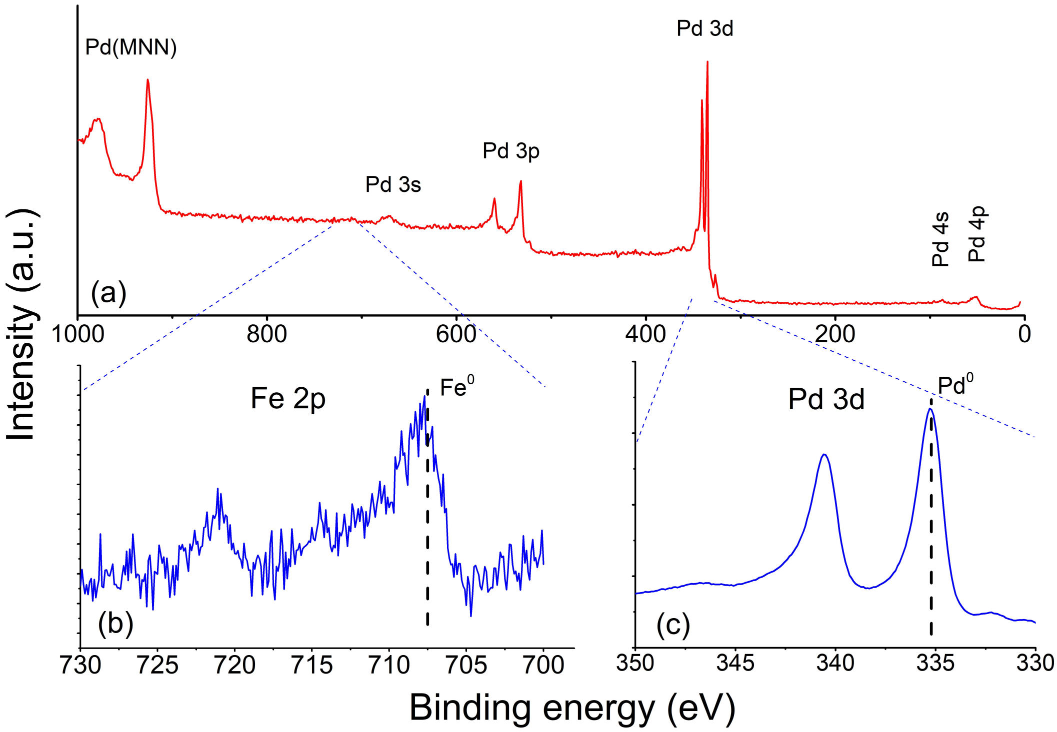

Figure 2. XPS survey spectrum of the topmost nominal $Pd_{0.96}Fe_{0.04}$ layer of the VN(15 nm)/$Pd_{0.96}Fe_{0.04}$(20 nm) heterostructure on MgO (a); high-resolution XPS-spectra in characteristic energy ranges for iron (b) and palladium (c).

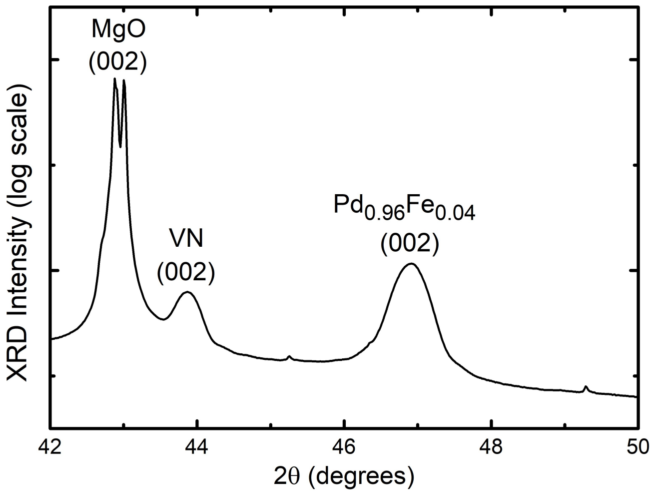

Figure 3. XRD pattern of the VN(15 nm)/$Pd_{0.96}Fe_{0.04}$(20 nm) heterostructure on the MgO (001) substrate.

3.3. Magnetometry and ferromagnetic resonance results

Magnetic properties of the VN/$Pd_{0.96}Fe_{0.04}$ thin-film heterostructure have been studied with the *dc* magnetometry and ferromagnetic resonance (FMR) spectroscopy techniques. Hysteresis loop measured with the magnetic field applied along the $\langle 100 \rangle$ in-plane direction of the MgO substrate is shown in Fig. 4. The shape of the loop suggests that this is the hard in-plane direction of the $Pd_{0.96}Fe_{0.04}$ film. Coercive field value is 0.8 mT, the saturation magnetization is 131 emu/cm^3. In Fig. 5 the FMR spectra of the VN/$Pd_{0.96}Fe_{0.04}$ heterostructure measured in the in-plane and out-of-plane geometries at two temperatures, 20 K and 5 K, are presented. At 20 K, the VN layer is in the normal state while, according to the conductivity measurements, at 5 K it is already in the superconducting state ($T_c \sim 5.2$ K, compare with the $T_{c0} \sim 7.85$ K of the same, uncapped with $Pd_{0.96}Fe_{0.04}$, vanadium nitride film). These results confirm the easy-plane character of the film magnetic anisotropy due to the dominating demagnetization field term [21–23]. An appearance of the wide microwave absorption in the low-field range is a consequence of the emerging superconductivity of the VN layer, its observations and mechanisms are discussed in Refs. [24–28]. Additional complexity may arise from the proximity ferromagnet/superconductor effect that evidently occurs in the studied heterostructure [29]. A bundle of sharp lines observed in the range of $300 - 400$ mT are the electron paramagnetic resonance signals originating from the $3d$-metal impurities in the MgO substrate.

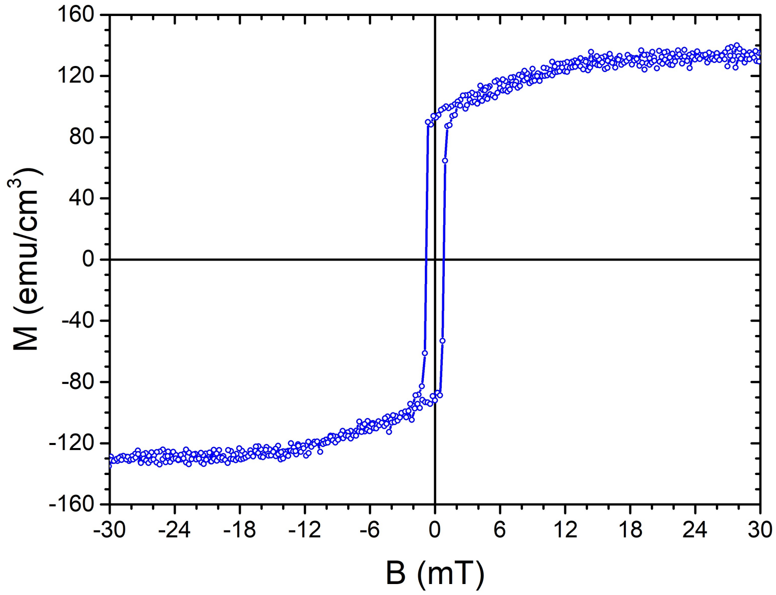

Figure 4. Magnetic hysteresis loop of the epitaxial VN/$Pd_{0.96}Fe_{0.04}$ thin-film heterostructure on the MgO (001) substrate measured along the $\langle 100 \rangle$ MgO in-plane direction; $T = 20$ K.

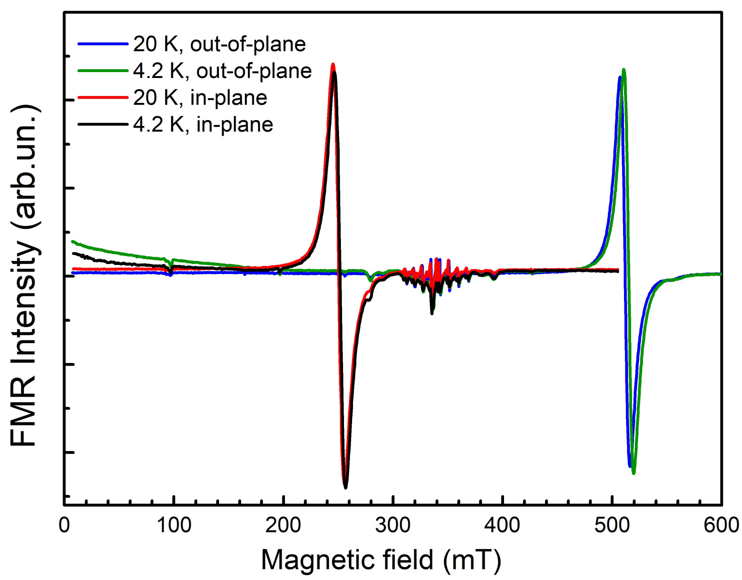

Figure 5. FMR spectra of the VN/$Pd_{0.96}Fe_{0.04}$ thin film heterostructure in the out-of-plane orientation $\mathbf{B}_0 \parallel [001]$ (the blue line for 20 K and the green one for 4.2 K), and with $\mathbf{B}_0 \parallel [100]$ lying in-plane (the red line for 20 K and the black one for 4.2 K); $\nu_{\mathrm{mw}} = 9.416$ GHz.

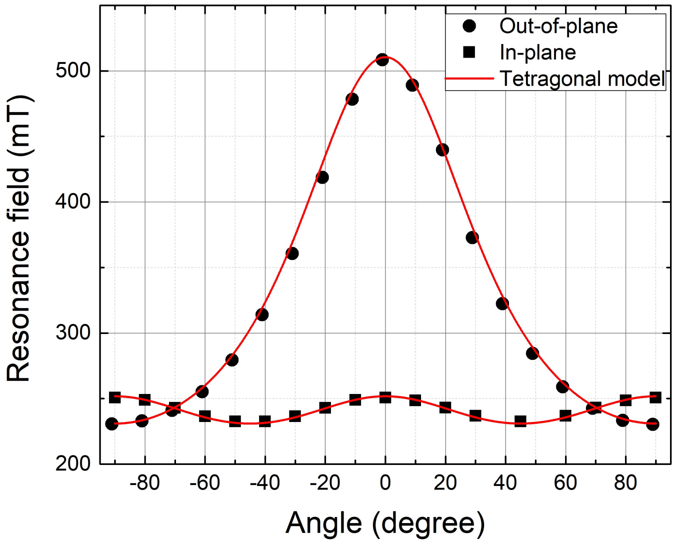

Figure 6. Angular dependence of the FMR resonance field of the epitaxial VN/Pd$_{0.96}$Fe$_{0.04}$ heterostructure for in-plane and out-of-plane geometries. Symbols illustrate experimental data; the solid red line is a fit that includes all the terms in the free energy density Eq. (1). For in-plane geometry rotation of the magnetic field was performed in the (110) plane of MgO with $\theta = 0$ corresponding to [001] direction; for in-plane geometry $\phi = 0$ corresponded to [100] direction of the substrate.

The angular dependence of the FMR field for resonance of the epitaxial VN/Pd$_{0.96}$Fe$_{0.04}$ heterostructure for the in-plane and out-of-plane geometries is shown in Fig. 6. Uniaxial two-fold symmetry is found for the out-of-plane sample rotation, while the four-fold symmetry is observed when the field is rotated in the film plane.

Orientation dependencies in Fig. 6 indicate also that the in-plane easy and hard axes for magnetization of the epitaxial Pd$_{0.96}$Fe$_{0.04}$ film within the VN/Pd$_{0.96}$Fe$_{0.04}$ heterostructure correspond to the $\langle 110 \rangle$ and $\langle 100 \rangle$ crystallographic directions of the MgO (001) substrate.

Anisotropy constants were extracted by simultaneous fitting of the in-plane and out-of-plane dependencies of the FMR resonance field using the free energy density expansion [21, 22]

$$E = -\mathbf{M} \cdot \mathbf{H} + 2\pi M_s^2 \alpha_3^2 - K_p \alpha_3^2 - \frac{1}{2} K_1 \left(\alpha_1^4 + \alpha_2^4 + \alpha_3^4 \right) - \frac{1}{2} K_2 \alpha_3^4. \tag{1}$$

The first term in the equation is the Zeeman energy in the external *dc* magnetic field **H**; the second term is the demagnetization energy related to the thin-film shape of the sample. The third term accumulates the "perpendicular" anisotropy coming from the interface with the substrate and the free surface, as well as a leading term of the tetragonal anisotropy. The last two terms are the cubic and the forth-order tetragonal anisotropy contributions, respectively.

Resonance field for a given direction of the applied magnetic field is found by simultaneous solution of the following equations [30, 31]:

$$\frac{dE}{d\phi} = 0, \qquad \frac{dE}{d\theta} = 0, \tag{2}$$

$$\omega_{\text{res}} = \frac{\gamma}{M_s \sin\theta} \left(E_{\theta\theta} E_{\phi\phi} - E_{\phi\theta}^2 \right)^{\frac{1}{2}}. \tag{3}$$

Equations (2) determine the equilibrium direction of the magnetic moment for a given direction and a magnitude of the *dc* magnetic field. Expression (3) is the Suhl equation for resonance, where $E_{\theta\theta}$, $E_{\phi\phi}$ and $E_{\phi\theta}$ are the second derivatives of the free energy Eq. (1) with respect to the magnetic moment direction angles, ϕ and θ; ω_{res} is the circular frequency of the spectrometer

Table 1. Parameters of the model of Eq. (1) obtained from the fits of the orientation dependences of the FMR resonance fields for 20 nm films of $Pd_{0.96}Fe_{0.04}$ deposited directly onto the MgO (001) substrate and onto the VN (15 nm) layer.

Sample	M_s, emu/cm^3	K_p, 10^4 erg/cm^3	K_1, 10^4 erg/cm^3	K_2, 10^4 erg/cm^3
VN/$Pd_{0.957}Fe_{0.043}$	131 ± 7	-0.01 ± 0.11	-0.94 ± 0.05	-1.87 ± 0.14
$Pd_{0.964}Fe_{0.036}$	119 ± 6	0.7 ± 0.5	-0.61 ± 0.05	-2.53 ± 0.14

oscillator, γ is the gyromagnetic ratio [30]. The number of the varied model parameters in the course of fitting was reduced by taking into account the value of $M_s = 131$ emu/cm^3 determined from the magnetometry data.

The parameters obtained by the fitting are given in Table 1. Also, in the second row of Table 1, the results of the study of the epitaxial $Pd_{0.962}Fe_{0.038}$(20nm) thin film on MgO (001) substrate [32] are shown for comparison. On the first sight, parameters obtained for the VN/$Pd_{0.96}Fe_{0.04}$ look contradictory: almost zero K_p value with non-zero K_2. This, however, is a consequence of a peculiar mutual compensation of the interface and magnetocrystalline contributions to the uniaxial-symmetry term of the free energy Eq. (1). As far as the comparison between the parameters for $Pd_{0.96}Fe_{0.04}$ film on MgO and on the VN layer are concerned, we find the forth-order cubic anisotropy constant K_1 for the latter notably larger while the forth-order tetragonal K_2 value is about 25 percent smaller. The difference in K_1 values we relate to the actual difference in iron concentrations of about 0.7% (see Ref. [32] for details). Decrease of the K_2 value, in our opinion, is due to a smaller lattice mismatch between Pd and VN than that for the Pd and MgO couple. Smaller lattice strains reduce the tetragonal distortion and related to them values of K_2 and K_p. Consequently, by comparing the table data, we conclude that VN and MgO substrates have a different effect on the thin film of palladium-rich $Pd_{1-x}Fe_x$ alloy due to a smaller mismatch of the $Pd_{1-x}Fe_x$ and VN lattice constants compared to $Pd_{1-x}Fe_x$ and MgO.

4. Summary

We have successfully grown the epitaxial VN (15 nm)/$Pd_{0.96}Fe_{0.04}$ (20 nm) thin film heterostructure on the MgO (001) substrate using the combination of the reactive magnetron sputtering and molecular beam epitaxy, which was confirmed by various structural analysis methods such as LEED, XRD, and FMR. Manifestations of the superconductivity are observed in both the in-plane and out-of-plane FMR spectra of the VN/$Pd_{0.96}Fe_{0.04}$ heterostructure at low temperature (4.2 K) that disappear with temperature increase to 20 K. The tetragonal distortion of the $Pd_{0.96}Fe_{0.04}$ on the VN layer is significantly reduced in comparison with $Pd_{0.96}Fe_{0.04}$ on MgO due to the reduced lattice mismatch.

Acknowledgments

The authors acknowledge support by the RSF, project No. 18-12-00459. R.V.Yu. acknowledges the support from the subsidy allocated to Kazan Federal University to fulfill the state assignment in the sphere of scientific activities (task No. 3.7704.2017/6.7).

References

1. Buzdin A.I. *Rev. Mod. Phys.* **77**, 935 (2005)
2. Eschrig M. *Rep. Prog. Phys.* **78**, 104501 (2015)
3. Bergeret F.S., Volkov A.F., Efetov K.B. *Rev. Mod. Phys.* **77**, 1321 (2005)

4. Vernik I.V., Bol'ginov V.V., Bakurskiy S.V., Golubov A.A., Kupriyanov M.Y., Ryazanov V.V., Mukhanov O.A. *IEEE Trans. Appl. Supercond.* **23**, 1701208 (2013)
5. Larkin T.I., Bol'ginov V.V., Stolyarov V.S., Ryazanov V.V., Vernik I.V., Tolpygo S.K., Mukhanov O.A. *Appl. Phys. Lett.* **100**, 222601 (2012)
6. Oh S., Youm D., Beasley M.R. *Appl. Phys. Lett.* **71**, 2376 (1997)
7. Held R., Xu J., Schmehl A., Schneider C.W., Mannhart J., Beasley M.R. *Appl. Phys. Lett.* **89**, 163509 (2006)
8. Gingrich E.C., Niedzielski B.M., Glick J.A., Wang Y., Miller D.L., Loloee R., Pratt W.P. Jr, Birge N.O. *Nat. Phys.* **12**, 564 (2016)
9. Baek B., Rippard W.H., Benz S.P., Russek S.E., Dresselhaus P.D. *Nat. Commun.* **5**, 3888 (2014)
10. Weides M., Kemmler M., Goldobin E., Koelle D., Kleiner R., Kohlstedt H., Buzdin A. *Appl. Phys. Lett.* **89**, 122511 (2006)
11. Ryazanov V.V., Bol'ginov V.V., Sobanin D.S., Vernik I.V., Tolpygo S.K., Kadin A.M., Mukhanov O.A. *Phys. Procedia* **36**, 35 (2012)
12. Ryazanov V.V., Oboznov V.A., Rusanov A.Y., Veretennikov A.V., Golubov A.A., Aarts J. *Phys. Rev. Lett.* **86**, 2427 (2001)
13. Oboznov V.A., Bol'ginov V.V., Feofanov A.K., Ryazanov V.V., Buzdin A.I. *Phys. Rev. Lett.* **96**, 197003 (2006)
14. Sellier H., Baraduc C., Lefloch F., Calemczuk R. *Phys. Rev. Lett.* **92**, 257005 (2004)
15. Feofanov A.K., Oboznov V.A., V.V. Bol'ginov, Lisenfeld J., Poletto S., Ryazanov V.V., Rossolenko A.N., Khabipov M., Balashov D., Zorin A.B. *Nat. Phys.* **6**, 593 (2010)
16. Bol'ginov V.V., Stolyarov V.S., Sobanin D.S., Karpovich A.L., Ryazanov V.V. *JETP Lett.* **95**, 366 (2012)
17. Esmaeili A., Yanilkin I.V., Gumarov A.I., Vakhitov I.R., Gabbasov B.F., Kiiamov A.G., Rogov A.M., Osin Y.N., Denisov A.E., Yusupov R.V. *Thin Solid Films* **669**, 338 (2019)
18. Ajami F.I., Maccrone R.K. *J. Phys. Chem. Solids* **36**, 7(1975)
19. Zhao B.R., Chen L., Luo H.L., Jack M.D., Mullin D.P. *Phys. Rev. B* **29**, 6198 (1984)
20. NIST X-Ray Photoelectron Spectroscopy Database, NIST Standard Reference Database Number 20, Version 4.1, National Institute of Standards and Technology, Gaithersburg, Maryland, USA, 2000, n.d.
21. Heinrich B., Cochran J.F. *Adv. Phys.* **42**, 523 (1993)
22. Farle M. *Rep. Progr. Phys.* **61**, 755 (1998)
23. Wuttig M., Liu X. *Ultrathin Metal Films: Magnetic and Structural Properties* in *Springer Science and Business Media* (2004)
24. Khachaturyan K., Weber E.R., Tejedor P., Stacy A.M., Portis A.M. *Phys. Rev. B* **36**, 8309 (1987)
25. Shaltiel D., Bill H., Grayevsky A., Junod A., Lovy D., Sadowski W., Walker E. *Phys. Rev. B* **43**, 13594 (1991)
26. Czyżak A., Stankowski J., Martinek J. *J. Phys. C: Supercond.* **201**, 379 (1992)

27. Shaltiel D. *J. Low Temp. Phys.* **130**, 383 (2003)

28. Shaltiel D., Krug von Nidda H.-A., Shapiro B.Y., Rosenstein B., Loidl A., Bogoslavsky B., Shapiro I., Fujii T., Watanabe T., Tamagai T. *J. Supercond. Nov. Magn.* **22**, 387 (2009)

29. Lenk D., Hemmida M., Morari R., Zdravkov V.I., Ullrich A., Müller C., Sidorenko A.S., Horn S., Tagirov L.R., Loidl A., Krug von Nidda H.-A., Tidecks R. *Phys. Rev. B* **93**, 184501 (2016)

30. Suhl H. *Phys. Rev.* **97**, 555 (1955)

31. Gurevich A.G., Melkov G.A. *Magnetization Oscillations and Waves*, Vol. 2, CRC Press, Boca Raton (1996), p. 445

32. Esmaeili A., Yanilkin I.V., Gumarov A.I., Vakhitov I.R., Gabbasov B.F., Yusupov R.V., Tagirov L.R. *J. Alloys Comp.* (2019) [submitted]